

Superconductor–Insulator Transition in Long MoGe Nanowires

Hyunjeong Kim, Shirin Jamali, and A. Rogachev

Department of Physics and Astronomy, University of Utah, Salt Lake City, Utah 84112, USA

(Dated: March 2, 2013)

Properties of one-dimensional superconducting wires depend on physical processes with different characteristic lengths. To identify the process dominant in the critical regime we have studied transport properties of very narrow (9-20 nm) MoGe wires fabricated by advanced electron-beam lithography in wide range of lengths, 1-25 μm . We observed that the wires undergo a superconductor–insulator transition that is controlled by cross sectional area of a wire and possibly also by the thickness-to-width ratio. Mean-field critical temperature decreases exponentially with the inverse of the wire cross section. We observed that qualitatively similar superconductor–insulator transition can be induced by external magnetic field. Some of our long superconducting MoGe nanowires can be identified as localized superconductors, namely in these wires one-electron localization length is much shorter than the length of a wire.

PACS numbers: 74.48.Na, 74.25.Dw, 74.40.+k

One-dimensional systems play a special role in physics since they often allow a more simple theoretical description than their counterparts in higher dimensions [1]. Moreover, experimental testing of 1D systems with finite length can probe the length scale of distinct physical processes. This possibility is particularly important for systems that have long-range coherence in 3D, such as superconductors. In a one-dimensional limit superconductivity can be suppressed by several processes. If a wire is microscopically disordered, enhanced Coulomb repulsion competes with the Cooper pairing and suppresses an amplitude of order parameter [2]. In a homogeneous wire this process determines mean-field critical temperature. Below this temperature, a superconducting wire can acquire resistance as a result of phase slips (PS), topological fluctuations of the order parameter. A phase slip can occur as a result of a thermally-activated fluctuation (TAPS) [4] or a quantum fluctuation (QPS) [3]. The activation barrier for both processes is the same and depends on the amplitude of the order parameter and coherence length. Recent theories suggest that the QPS rate can also depend on some long-scale (or external) parameters. For example the QPS rate can be suppressed both in wires shorter than the length of the phase propagation during a phase slip [5] and in very long wires as a result of attractive interaction between QPS with different signs [6]. The quantum state of a wire is also predicted to depend on the state [7] and impedance [8] of macroscopic electrodes connected to a wire and on coupling to a dissipative environment [9–11].

Experimentally, there are at least two unusual effects that cannot be explained by local physics. One of them is the anti-proximity effect in Zn [12] and Al [13] nanowires. The other is superconductor–insulator transition (SIT) in short MoGe nanowires [14, 15] (length 30-300 nm), which is claimed to be controlled by the *normal state resistance* of a wire with separatrix set by $R_Q = 6.45 \text{ k}\Omega$. No QPS was detected in this work. Surprisingly, experi-

ments on longer MoGe wires [16] did not reveal the SIT; instead a crossover between superconducting and insulating variations was observed and interpreted in terms of the increasing rate of unbound QPS. It was suggested that the discrepancy between the behavior of short and long MoGe nanowires indicates the existence of a characteristic wire length separating the SIT and crossover regimes [5, 17]. The QPS contribution and crossover behavior were also detected in long PbIn [18], Nb [19] and Al [20, 21] nanowires.

Experimental studies of 1D superconductors face a technical challenge of fabricating ultra-narrow *homogeneous* wires. For amorphous MoGe alloys, this was previously achieved by deposition of MoGe on top of suspended carbon nanotubes. With this method, known as the molecular templating technique [17], wires with width down to 8 nm were fabricated and measured. Disadvantage of the method is that a wire can not be made sufficiently long; typically, the length is limited (depending of a type of carbon nanotubes) by 0.3 - 1 μm .

In the present work, we use an alternative fabrication method – high resolution electron beam lithography with negative resist [22, 23]. The technique is advanced; in experiments testing its resolution limit, we were able to fabricate lines with the width of about 6 nm. Figure 1A shows a scanning electron microscopy image of one of the nanowires with the width below 10 nm used in transport measurements. The method does not have the length limitation. Another advantage is a possibility to make samples with a true 4-probe geometry as shown in Fig. 1C. In these samples, current electrodes, voltage probes and a wire are fabricated simultaneously from the same original MoGe films. The procedure produces smooth connections between electrodes and wires as shown in Figs. 1A and 1B. We fabricated and studied two series of nanowires from amorphous alloys with a distinct relative content of Mo and Ge: $\text{Mo}_{78}\text{Ge}_{22}$ and $\text{Mo}_{50}\text{Ge}_{50}$. Details of nanowire fabrication and measurements are given in

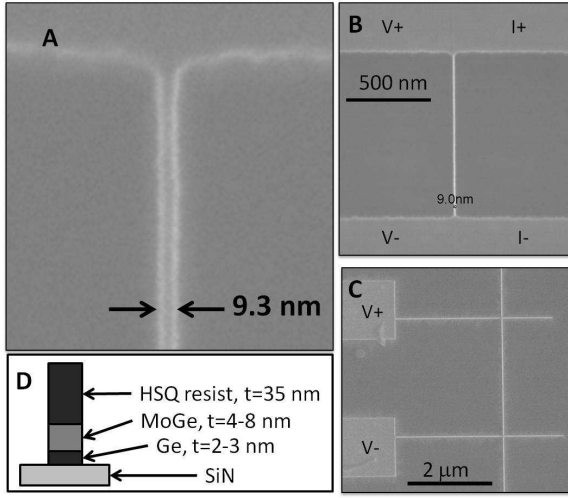


FIG. 1: Sample geometry. (A) Scanning Electron Microscopy image of a nanowire fabricated by high-resolution electron beam lithography with negative HSQ resist. Connection to a film electrode is shown on the top of the figure. (B) Electrodes geometry for quasi-4-probe transport measurements used in majority of samples. (C) Electrodes geometry for 4-probe measurements with voltage-probe electrodes made of nanowires. Current electrodes are outside of the image. (D) Sketch of the cross section of a typical sample.

supplementary materials [24]. Figure 1D schematically shows the cross section of a sample.

The parameters of $\text{Mo}_{78}\text{Ge}_{22}$ nanowires are summarized in Table 1. The resistance of the wires increases by few percent when temperature decreases from 300 K down to 2-4 K. This behavior is typical for strongly disordered systems; the gain in resistance is due to the weak localization and electron-electron interaction corrections [25]. The actual cross section area of nanowires, A , is not exactly known. The thickness of a wire is reduced from its nominal value (typically by 0.5-1 nm) due to oxidation and etching by the TMAH developer [24]. As shown in Fig. 1D, a MoGe nanowire is permanently covered by a 35-nm thick layer of exposed HSQ e-beam resist. However, the sides of a wire are not protected so the actual width of a wire can be reduced as a result of oxidation. Fortunately, MoGe films are known to have constant volume resistivity ($\rho = 160 \mu\Omega \text{ cm}$) down to thickness of 1 nm [28]. This property allows us to estimate cross sectional area as $A = \rho L / R_{RT}$, where L is wire length and R_{RT} is resistance at $T=300 \text{ K}$.

In Fig. 2 we plot resistance per unit length, $\rho_L(T) = R(T)/L$, at low temperatures for a series of $\text{Mo}_{78}\text{Ge}_{22}$ nanowires. The wires are labeled by letters and their length in micrometers is indicated in the parentheses. All wires can be clearly separated in two groups: superconducting and insulating. Insulating wires (labeled as M, L, J) have resistance monotonously decreasing with temperature. As shown in Fig 2B, conductance in these

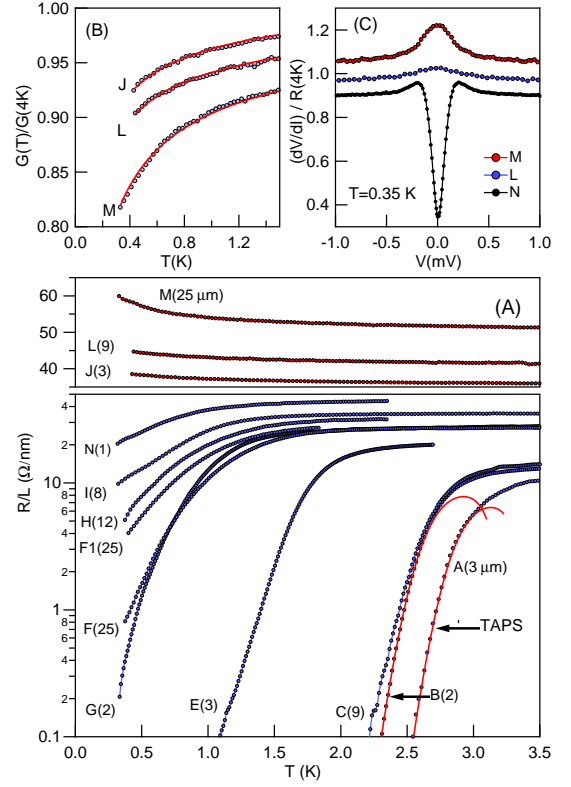


FIG. 2: Superconductor-insulator transition in zero-magnetic field. (A) Resistance over length versus temperature for a series of $\text{Mo}_{78}\text{Ge}_{22}$ nanowires. Letters label the nanowires and numbers in the brackets indicate the nanowire lengths in micrometers. For wires A and B, solid red lines are the fitting curves to the theory of thermally activated phase slips. (B) Low-bias conductance normalized by the value of conductance at 4 K as a function of temperature for insulating wires. Solid red lines are the fitting curves to the theory of electron-electron interactions in 1D. Data for wires L and M are downshifted by 0.02 and 0.04, respectively. (C) Normalized differential resistance at $T=0.35 \text{ K}$ for indicated wires. Data for wires L and N are downshifted by 0.05 and 0.1, respectively.

wires can be well fitted by the dependence $G(T) = G_0 - \alpha/\sqrt{T}$ accounting for the electron-electron interaction in a normal disordered one-dimension metal (eq. 5.5 in Ref.[25]). The one-dimensional approximation is valid when the width of a wire is smaller than the thermal length $L_T = \sqrt{\hbar D / k_B T}$ [25]. With the diffusion coefficient of $\text{Mo}_{78}\text{Ge}_{22}$, $D = 0.5 \text{ cm}^2\text{s}^{-1}$ [26], this approximation is satisfied for our insulating wires below 1.5 K. The presence of the SIT is also evident from nonlinear differential resistance shown in Fig 2C (data were taken at $T=0.35 \text{ K}$). The wires always show zero-bias anomaly that changes from negative to positive when the system crosses the SIT.

The lower panel in the Fig. 2A shows $\rho_L(T)$ for superconducting wires. We observed that as the resistance per

	t (nm)	w (nm)	L (μ m)	R_{RT} (k Ω)	R_{LT} (k Ω)	$\rho_L(300\text{ K})$ (Ω/nm)	A (nm^2)	T_c (K)
A	7	25	3	33	34.5	11	145	3.0
B	8	19	2	26	28	13	123	2.7
C	7	21	9	125	132	14	115	2.7
E	7	20	3	59	62	20	81	1.8
F	7	15	25	630	680	25	64	1.1
G	6	17	2	51	56	26	63	1.0
F1	7	15	25	680	730	27	59	0.9
H	7	14	12	356	381	30	54	0.8
I	6	10	8	251	282	31	51	0.6
N	6	9	1	43	45	43	37	0.3
J	4	17	3	90	106	30	53	0
K	4	17	18	650	740	36	44	0
M	4	15	25	1150	1300	46	35	0

TABLE I: The experimental parameters characterizing $\text{Mo}_{78}\text{Ge}_{22}$ nanowires: t – nominal thickness; w – nominal width obtained from an SEM image of a wire; L – length; R_{RT} – resistance at room temperature; R_{LT} – resistance at low temperature (2-4 K); $\rho_L = R_{RT}/L$ – resistance per length at room temperature; A – effective cross section area estimated as $A = \rho L/R_{RT}$, where $\rho=160\text{ }\mu\Omega\text{cm}$ is the bulk resistivity of $\text{Mo}_{78}\text{Ge}_{22}$ amorphous alloy; T_c – critical temperature taken at the midpoint of a superconducting transition.

length in the normal state increases the superconducting transition progressively shifts to low temperatures. Because the cross sectional area, A , of MoGe nanowires is inversely proportional to $\rho_L(300\text{K})$ and in the normal state $\rho_L(T)$ depends on temperature weakly, we can conclude that superconducting transition in MoGe nanowires is controlled by A . From Table 1 one may notice that the cross sectional area of insulating wires J and K is larger than that of superconducting wire N. Wire N has width 9 nm and is the narrowest wire we have measured. It is possible that this wire has granular structure as a result of non-uniform side oxidation. However we may also notice that wire J has nominal cross section $4\times 17\text{ nm}^2$ and wire N $6\times 9\text{ nm}^2$. So the alternative explanation is to assume that the cross sectional area is not the only parameter controlling the SIT and that for wires with the same A , the superconductivity is stronger when thickness-to-width ratio is closer to one. Qualitatively similar behavior was observed in wide MoGe stripes [26].

We do not find any evidence that the length of a wire or its normal state resistance plays any role in setting superconductivity. This is further confirmed by measurements on wires A, C, and J that have 4-probe electrode geometry shown in Fig. 1C. We found no difference in measurements done in quasi-4-probe (Fig. 1B) and 4-probe geometry, which implies that superconductivity in MoGe wires is not influenced by electrodes.

Our set of long superconducting wires allows us to make an interesting observation. The Anderson localization theory predicts that one-electron states in a disordered normal wire decay exponentially with a localization length that can be estimated as $\xi_A = 2Ak_F^2\ell/3\pi^2$ [27]. Following Ref. [28], we use for a mean free path a value $\ell=0.3\text{ nm}$ and estimate the Fermi vector k_F from the free-electron equation for volume resistivity,

$1/\rho = (e^2k_F^2\ell)/(3\pi^2\hbar)$, which gives $k_F=1.6\text{ }\text{\AA}^{-1}$. With these parameters we estimate for wire F that $\xi_A \approx 300\text{ nm}$, which is much smaller than the length of the wire. Therefore, wire F (as well as several other wires) can be identified as a *localized superconductor*. The term, introduced by Ma and Lee [29], describes a system in which superconducting pairing occurs between time-reversed localized one-electron states. Our observations suggest that the long-range behavior of one-electron wave functions is not important for setting superconductivity in long disordered nanowires.

In a 1D superconductor, the finite width of the superconducting transition arises due to phase slips. For our thickest wires A,B and C, the $\rho_L(T)$ dependence can be well-explained by the theory of thermally-activated phase slips (TAPS), as shown in Fig. 2A (we followed the fitting procedure given in Refs.[16] and [30]). Fitting parameters (T_c and the zero-temperature Ginzburg-Landau coherence length $\xi(0)$) are $T_c=3.4\text{ K}$, $\xi(0)=9\text{ nm}$ for wire A and $T_c=3.2\text{ K}$, $\xi(0)=9\text{ nm}$ for wire B. For wires with smaller cross sectional area, fitting with the TAPS theory is not satisfactory and returns unreasonably high values of T_c and $\xi(0)$. This trend, observed also in short MoGe [31] and Nb [32] nanowires, possibly reflects a proximity to a zero-temperature quantum phase transition, where $\xi(0)$ is expected to diverge. The deviation from the TAPS behavior could be due to an additional contribution from unbound quantum phase slips. However, for all our superconducting wires we observe a single-step transition without any characteristic features of QPS process such as a “tail” or positive curvature in $\rho_L(T)$ curves, or saturation to a constant resistivity at low temperatures. Our data are markedly different from the results on series of MoGe nanowires reported by Lau *et al.*[16], where the QPS contribution was used to explain behavior of $\rho_L(T)$

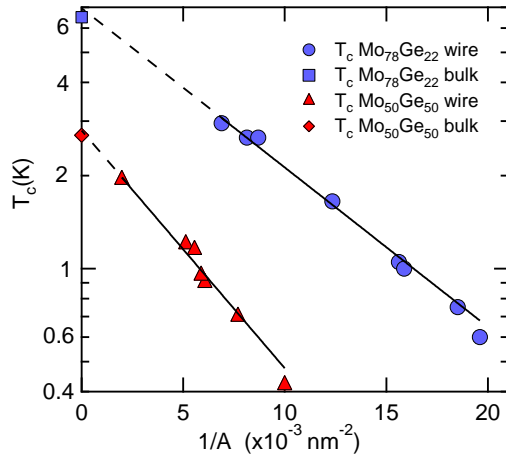


FIG. 3: Critical temperature of $\text{Mo}_{78}\text{Ge}_{22}$ and $\text{Mo}_{50}\text{Ge}_{50}$ nanowires as a function of the inverse of the wire cross sectional area. Solid lines represent a simple exponential form. The dashed lines indicate the extension of the exponential dependence to the $1/A = 0$. Squares indicate the critical temperature of corresponding bulk alloys.

dependence.

We can also compare our results with the large set of data on short $\text{Mo}_{78}\text{Ge}_{22}$ nanowires fabricated by the molecular template technique with length in the range 30-300 nm reported by Bollinger *et al.* [15]. All wires in this set do not show evidence for the QPS or crossover behavior; instead, a direct superconductor-insulator transition was observed with a separatrix set by total wire resistance equal to $R_Q = 6.45$ k Ω . The main evidence for this observation comes from wires with length smaller than 100 nm. At low temperatures superconductivity in these wires can be possibly affected by the proximity effect because of the attached superconducting electrodes. We found that, if nanowires with length smaller than 100 nm are excluded, the data provided by Bollinger match well the data for our long nanowires when plotted in the $\rho_L(T)$ form. Both sets show a progressive shift of T_c with decreasing cross sectional area, approximately the same width of superconducting transitions and the same critical value of $\rho_L \approx 40$ Ω/nm separating insulating and superconducting regimes. Combined data cover the range from 100 nm to 25 μm clearly indicating that there is no length discrepancy in the behavior of $\text{Mo}_{78}\text{Ge}_{22}$ nanowires.

For each our wire we can define the empirical mean-field critical temperature, T_c , by choosing it in the middle of the transition. T_c is plotted in Fig. 3 on a logarithmic scale as a function of the inverse of the wire cross sectional area, $1/A$, for two series of wires fabricated from amorphous $\text{Mo}_{78}\text{Ge}_{22}$ and $\text{Mo}_{50}\text{Ge}_{50}$ alloys. For $\text{Mo}_{50}\text{Ge}_{50}$ the cross sectional area A was computed from

$A = \rho L / R_{RT}$, with $\rho = 235$ $\mu\Omega\text{cm}$ determined in separate measurements on film samples. Remarkably, the data for both series can be fitted by a simple exponential dependence $T_c = T_{c0} \exp(-\beta/A)$, shown as a solid line in the figure. The fitting parameter T_{c0} agrees with the indicated bulk critical temperature of the corresponding alloy. The second fitting parameter is $\beta = 120$ nm^2 for $\text{Mo}_{78}\text{Ge}_{22}$ and $\beta = 180$ nm^2 for $\text{Mo}_{50}\text{Ge}_{50}$.

Suppression of T_c by disorder-enhanced Coulomb repulsion was analyzed theoretically for the crossover region from 2D to 1D [2, 33], and the theory was used to explain the behavior of T_c in Pb stripes [34]. Similar to our observation the fermionic theories predict an exponential suppression of T_c ; however, there is a big quantitative disagreement with our data. For example, we observe experimentally that for a $\text{Mo}_{78}\text{Ge}_{22}$ wire A with an estimated thickness 6 nm and sheet resistance $R_\square \approx 230$ Ω , reduction of the width from infinity (2D limit) to 25 nm reduces the critical temperature by 45 %, from 5.5 to 3 K. On the other hand, when we followed numerical routines given in Ref.[2] we found that essentially no T_c reduction is expected for this wire. The discrepancy can also be noticed directly from a comparison with the experimental data on the Pb stripe with width 22 nm that, unlike the MoGe wire, show no detectable T_c reduction compared to the 2D case [34]. The fermionic theories we used for the analysis do not include the effect of the Coulomb interaction on the single-particle density of states. Adding this contribution, as it was done previously for MoGe films [35], may perhaps improve an agreement with the experiment.

An alternative way to explain the strong deviation of T_c from the fermionic theory is to assume that $\rho_L(T)$ dependencies are modified and shifted to lower temperatures by *interacting* quantum phase slips as was suggested theoretically in Refs. [6] and [5]. These processes, at least in principle, could also explain the appearance of the zero-bias anomaly in the insulating wires and functional behavior of $\rho_L(T)$ in thin superconducting wires, where it deviates from the TAPS theory but nevertheless has negative curvature. However, the overall shift in T_c produced by the interacting QPSs is expected to depend on a wire length. The lack of any dependence of T_c on the length on MoGe wires brings strong argument against the relevance of the interacting QPSs to our system.

To clarify this question further we studied the suppression of superconductivity in thin wires by magnetic field. The variation of the resistivity of wire F1 at different magnetic fields (applied normal to the wire and substrate) is shown in Fig. 4A. Comparison of the data shown in Figs. 2 and 4 indicates that the evolution of the resistance in the critical regime both as a function of temperature and voltage bias is qualitatively the same for transitions driven by the magnetic field or reduction of cross sectional area. In both cases, the transition from superconducting to insulating behavior in $\rho_L(T)$ curves is

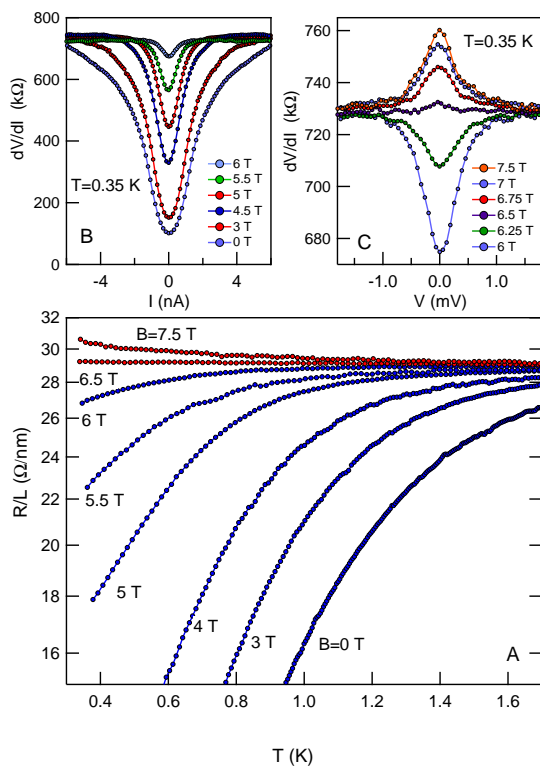


FIG. 4: Superconductor-insulator transition driven by magnetic field. (A) Temperature dependence of resistance per unit length for a nanowire F1 at indicated magnetic fields. (B) Differential resistance as function of current at $T=0.35$ K in superconducting regime at indicated magnetic fields. (C) Differential resistance as a function of bias voltage at $T=0.35$ K in the transitional regime of the SIT.

accompanied by the sign change of the zero-bias anomaly (ZBA) in differential resistance as shown in Fig. 4C. It is likely that in both cases the same physics controls the critical regime of the SIT. For superconducting wires far from the critical field the narrowing of the ZBA with increasing magnetic field (shown as a function of current in Fig. 4B) simply reflects the decrease of the critical current of a wire. The origin of the ZBA in insulating and transitional regimes is not well understood.

One-dimensional superconductors are too thin to allow formation of vortices; instead, magnetic field uniformly penetrates a wire and suppresses the amplitude of the order parameter acting on the orbital and spin part of a Cooper pair. The suppression of superconductivity by a magnetic field in one-dimension is a local fermionic process. Using parameters of nanowire F1 (mean-field $T_c = 0.9$ K, estimated width $w = 10$ nm, diffusion coefficient $D = 0.5$ cm²/s [26], spin-orbit scattering time $\tau_{so} \approx 5 \times 10^{-14}$ s [30]) we can estimate suppression of T_c from standard formulas for the orbital ($\alpha_o = Dw^2e^2B^2/6\hbar$) and spin ($\alpha_s = \hbar\tau_{so}e^2B^2/2m^2$) pair-breakers [4]. Since both contributions are quadratic in a magnetic field we

used the formula $1.76k_B T_c = 2\alpha = 2(\alpha_o(B_c) + \alpha_s(B_c))$ and found that $B_c \approx 6$ T. It agrees with the experimental value $B_c \approx 6.5$ T. The agreement suggests that the zero-field T_c even for our thinnest wires should be interpreted as a usual mean-field critical temperature reflecting the reduced magnitude of the order-parameter.

In summary, we observed the superconductor-insulator transition in a series of long MoGe nanowires. The SIT, that likely has fermionic nature, can be driven by wire cross section and by magnetic field.

The authors thank A.M. Finkel'stein, L.B. Ioffe, E.G. Mishchenko, D. Mozyrsky, Y. Oreg, and M.E. Raikh for valuable discussions and B. Baker, M.C. DeLong, and R.C. Polson for technical support. Sample fabrication was carried out at the University of Utah Microfab and USTAR facilities. This work is supported by NSF CAREER Grant DMR 0955484.

-
- [1] T. Giamarchi, *Quantum Physics in One Dimension*, Oxford: New York (2004).
 - [2] Y. Oreg and A.M. Finkelstein, Phys. Rev. Lett. **83**, 191 (1999).
 - [3] K.Y. Arutyunov, D.S. Golubev, and A.D. Zaikin, Phys. Rep. **464**, 1-70 (2008).
 - [4] M. Tinkham, *Introduction to Superconductivity*, 2nd ed.; McGraw-Hill: New York (1996).
 - [5] D. Meidan, Y. Oreg, and G. Refael, Phys. Rev. Lett. **98**, 187001 (2007).
 - [6] A.D. Zaikin, D.S. Golubev, A. va Otterlo, and G.T. Zimanyi, Phys. Rev. Lett. **78**, 1552 (1997).
 - [7] S. Sachdev, P. Werner, and M. Troyer, Phys. Rev. Lett. **92**, 237003 (2004).
 - [8] S. Khlebnikov, Phys. Rev. B **77**, 104505 (2008).
 - [9] H.P. Buchler, V.B. Geshkenbein, and G. Blatter, Phys. Rev. Lett. **92**, 067077 (2004).
 - [10] J.A. Hoyos, C. Kotabage, and T. Vojta, Phys. Rev. Lett. **99**, 230601 (2007).
 - [11] H.C. Fu, A. Seidel, J. Clarke, and D.-H. Lee, Phys. Rev. Lett. **96**, 157005 (2006).
 - [12] M. Tian, N. Kumar, S. Xu, J. Wang, J.S. Kurtz, and M.H.W. Chan, Phys. Rev. Lett. **95**, 076802 (2005).
 - [13] M. Singh, J. Wang, M. Tian, T.E. Mallouk, and M.H.W. Chan, Phys. Rev. B **83**, 220506 (2011).
 - [14] A. Bezryadin, C.N. Lau, and M. Tinkham, Nature **404**, 971 (2000).
 - [15] A.T. Bollinger, R.C. Dinsmore III, A. Rogachev, and A. Bezryadin, Phys. Rev. Lett. **101**, 227003 (2008).
 - [16] C.N. Lau, N. Markovic, M. Bockrath, A. Bezryadin, and M. Tinkham, Phys. Rev. Lett. **87**, 217003 (2001).
 - [17] A. Bezryadin and P.M. Goldbart, Adv. Mater. **22**, 1111-1121 (2010).
 - [18] N. Giordano and E.R. Schuler, Phys. Rev. Lett. **63**, 2417 (1989).
 - [19] K. Xu and J.R. Heath, Nano Lett. **8**, 136 (2008).
 - [20] F. Altomare, A.M. Chang, M.R. Melloch, Y. Hong, and C.W. Tu, Phys. Rev. Lett. **97**, 017001 (2006).
 - [21] M. Zgrinski, K.-P. Riikonen, V. Touboltsev, and K. Arutyunov, Nano Lett. **5**, 1029-1033 (2005).

- [22] H. Namatsu *et al.*, J. Vac. Sci. Technol. B, **16**, 69 (1998).
- [23] J.K.W. Yang *et al.* J. Vac. Sci. Technol. B **27** 2622 (2009).
- [24] Supplementary materials.
- [25] B.L. Altshuler and A.G. Aronov, in *Electron-Electron Interaction in Disordered Systems*, eds. A.L. Efros and M. Pollak, Elsevier Science Publ. (1985).
- [26] J.M. Graybeal, P.M. Mankiewich, R.C. Dynes, and M.R. Beasley, Phys. Rev. Lett. **59**, 2697 (1987).
- [27] D.J. Thouless, Phys. Rev. Lett. **39**, 1167 (1977).
- [28] J.M. Graybeal, PhD thesis, Stanford University (1985).
- [29] M. Ma and P.A. Lee, Phys. Rev. B **32**, 5658 (1985).
- [30] A. Rogachev, A.T. Bollinger, and A. Bezryadin, Phys. Rev. Lett. **94**, 017004 (2005).
- [31] A. Rogachev, T.-C. Wei, D. Pekker, A.T. Bollinger, P.M. Goldbart, and A. Bezryadin, Phys. Rev. Lett. **97**, 137001 (2006).
- [32] A. Rogachev and A. Bezryadin, Appl Phys. Lett. **83**, 512-514 (2003).
- [33] R.A. Smith, B.S. Handy, and V. Ambegaokar, Phys. Rev. B **63**, 094513 (2001).
- [34] F. Sharifi, A.V. Herzog, and R.C. Dynes, Phys. Rev. Lett. **71**, 428 (1993).
- [35] T.R. Kirkpatrick and D. Belitz, Phys. Rev. Lett. **68**, 3232 (1992).

Supplementary materials.

1. Nanowire fabrications. The nanowires were fabricated using Si wafers covered with a 100 nm layer of SiN and cut in individual samples with size $6 \times 9 \text{ mm}^2$. First, using optical photolithography, consequential deposition of Ti (20 nm) and Au (40 nm) films, and lift-off procedure we fabricated a pattern consisting of 12 electrodes and several markers. The markers were later used for alignment and focusing during electron beam lithography. Next, we sputter deposited a layer of amorphous Ge (thickness 3 nm) followed (without breaking vacuum) by the sputter deposition of MoGe alloy (thickness 4-8 nm). The Ge underlayer helped to produce uniform MoGe films. To make good electrical connection between pre-

patterned Ti/Au electrodes and thin MoGe films, square pads (5×5 micrometers, thickness 30 nm) were placed in each contact area by positive electron beam lithography with PMAA and liftoff. After patterning contact pads, the sample was immersed in the 2.5 % water solution of TMAH (the developer for negative electron beam lithography) for clearing. It was realized that TMAH slightly etches MoGe films with average rate of about 0.2 nm/min. In the next stage the whole sample was spin coated with 35-nm thick HSQ (hydrogen silsequioxane) layer. The speciation of the solution is XR-1541 2 %; it was purchased from Dow Corning. The nanowire and film electrodes (shown in Fig. 1 of the main text) were patterned by electron-beam lithography in Nova Nano 630 Scanning Electron Microscope with standard field-emission Schottky gun and the NPJS package for beam control. The accelerating voltage was 30 keV; the dosage was 400-600 $\mu\text{C}/\text{cm}^2$ for area and 3-8 nC/cm for lines. The exposed pattern was developed in 2.5 % water solution of TMAH for 2 min to remove HSQ that was not exposed to the e-beam (negative lithography). The pattern was etched with reactive ion etching using SF_6 gas. The exposed HSQ resist permanently remains on top of a wire and electrodes. To prevent oxidation the wires were stored under vacuum.

2. Noise filtering. Transport measurements were carried out in a He-3 cryostat. Each line at room temperature was interrupted by a Pi-filter with cutoff frequency of 1 MHz. The design of low-temperature filters was copied from the Marcus group at Harvard University (A.C. Johnson, Appendix C, PhD thesis 2006, Harvard University). In each line, we added three 100 Ω resistors connected in series and tightly anchored into three separate brass plates. Silver paste was used to seal the resistors in the brass plate.